# Performance Analysis of Protograph LDPC Codes Over Large-Scale MIMO Channels With Low-Resolution ADCs

**THUY V. NGUYEN[1], HIEU D. VU[1], DIEP N. NGUYEN [ID]2, AND HIEU T. NGUYEN [ID]3**

[1]Faculty of Information Technology, Posts and Telecommunications Institute of Technology, Hanoi 10000, Vietnam
[2]School of Electrical and Data Engineering, University of Technology Sydney, Ultimo, NSW 2007, Australia
[3]Department of Science and Industry Systems, Faculty of Technology, Natural Sciences and Maritime Sciences, University of South-Eastern Norway, 3603 Kongsberg, Norway

Corresponding author: Hieu T. Nguyen (hieu.nguyen@usn.no)

**ABSTRACT** Protograph LDPC (P-LDPC) codes and large-scale multiple-input multiple-output (LS-MIMO) are cornerstones of 5G and future wireless systems, thanks to their powerful error-correcting capability and high spectral efficiency. To alleviate the high complexity in signal detection/decoding that dramatically grows with the number of antennas (in the order of tens or even hundreds), low-resolution analog-to-digital converters (ADCs) and joint detection and decoding using factor graph have recently attracted paramount interest. Unlike high-resolution ADCs, by using a small number of bits to quantize the received signal, low-resolution ADCs help reduce the hardware cost and power consumption of the RF circuit of practical LS-MIMO transceivers. Such a very much desirable reduction comes at the cost of additional quantization noise, introduced by low-resolution ADCs. This work aims to provide a unified framework to analyze the impact of the low-resolution ADCs on the performance of P-LDPC codes in practical LS-MIMO systems. It is worth noting that the previous analytical tools that have been used to evaluate the performance of P-LDPC codes do not account for the quantization noise effect of the low-resolution ADCs and the fact that the covariance of quantization noise depends on the fading channels. This article addresses this shortcoming by first leveraging the additive quantization noise model. We then derive the expression of extrinsic information for the belief-propagation LS-MIMO detector. The mutual information functions, which are the core elements of our proposed protograph extrinsic information transfer (PEXIT) algorithm, are analyzed for LS-MIMO communication systems. Our proposed PEXIT algorithm allows us to analyze and predict the impact of the low-resolution ADCs on the performance of P-LDPC codes, considering various input parameters, including the LS-MIMO configuration, the code rate, and the maximum number of decoding iterations, and the code structure. Based on our extensive analytical and simulation results, we found that the performance of 3-bit and 4-bit ADC systems only have a small gap to that of the unquantized systems. Especially when the 5-bit ADC scheme is applied, the performance loss is negligible. This finding sheds light on the practical design of LS-MIMO systems using P-LDPC codes.

**INDEX TERMS** Protograph LDPC codes, large-scale MIMO, joint detection and decoding, PEXIT algorithm, low-resolution ADC.

## I. INTRODUCTION

### A. MOTIVATION

Both protograph LDPC (P-LDPC) codes[1] and large-scale MIMO (LS-MIMO) have attracted considerable interest and

The associate editor coordinating the review of this manuscript and approving it for publication was Xueqin Jiang [ID].

[1]A P-LDPC code is defined by a small bipartite graph, so-called a protograph [1]. From the small graph, a larger derived graph is built to form a practical LDPC code by applying a "copy-and-permutation" operation.

found their applications in 5G and future wireless systems. This is thanks to LDPC's powerful error-correcting capability and low complexity encoder/decoder structures [2] that can be adapted to the joint detection and decoding using factor graphs in LS-MIMO [3]–[8]. To simultaneously reap up the advantages of both P-LDPC and LS-MIMO, one needs to address the complexity of their signal detection and decoding - that dramatically grows with the number of antennas (in the order of tens or even hundreds in LS-MIMO).

This large number of antennas used in LS-MIMO systems gives rise to technical challenges at both the radio frequency (RF) module and the baseband signal processing stage. At the RF interface, using multiple pairs of the analog-to-digital converter (ADC) and digital-to-analog converter (DAC) at the receiver side increases not only the hardware cost but also the power consumption since the hardware cost and the power consumption of ADCs and DACs grow linearly with the bandwidth and exponentially with the number of quantization bits, respectively. For that, an attractive solution is to replace the power-hungry high-resolution ADCs with low-power low-resolution ADCs (see [9] and references therein). At the based band signal processing stage, conventional signal detectors, e.g., the maximum likelihood detection (MLD) [10]–[12] that is often regarded as the most powerful detection scheme for the conventional MIMO system with 2-8 antennas is not computationally pragmatic. Since the complexity of this detector grows exponentially with the number of antennas [11], these detectors are no longer suitable for LS-MIMO systems with tens or hundreds of antennas. To circumvent the complexity issue, the joint detection and decoding based on the factor graph has been proposed as an attractive alternative [4], [12].

Given the above, this work aims to propose a unified framework to analyze the impact of the low-resolution ADCs on the performance of the P-LDPC codes used in LS-MIMO communication systems.

### B. RELATED WORKS

To design and evaluate the performance of P-LDPC codes, one often relies on the original protograph extrinsic information transfer (PEXIT) algorithm (using the iterative decoding threshold). Nguyen *et al.* [13], applied the original PEXIT algorithm, which was derived for AWGN channels [14], to design NND code, which obtains the coding gain over the classical AR4JA code by Divsalar *et al.* [15]. Authors in [16] introduced a modified version of the PEXIT algorithm in [14] for spatial diversity communication systems. However, this PEXIT variant is only applicable to the conventional MIMO systems with the space-time code and receiving diversity schemes. It does not apply to LS-MIMO communications systems where the message-passing joint detection and decoding algorithm is employed.

In [4], authors applied the standard extrinsic information transfer (EXIT) chart proposed in [17] to design the irregular LDPC codes for LS-MIMO channels. By optimizing both variable and check degree distributions, a resulting code achieves significant coding gain, up to 1.8 dB, over the previous off-the-shelf codes. Even though the framework in [4] is derived for the joint message-passing detection and decoding for LS-MIMO channels, the EXIT algorithm used in [4] is not suitable for the protograph codes [14]. In addition, none of the previous versions of the EXIT algorithm considered the impact of low-resolution ADCs on protograph LDPC codes in LS-MIMO channels. Unlike high-resolution LDPC LS-MIMO systems, e.g., [4], the low-resolution ADCs incurs

quantization noise whose covariance also depends on the fading channels.

To overcome the drawbacks of the previous frameworks, this work aims to study the impact of low-resolution ADCs whose quantization noise is often modeled as additive noise in quantized MIMO systems (see [5], [7] and therein references). To that end, we adopt the iterative joint detection and decoding algorithm and the soft interference cancellation (instead of the maximum ratio combining in earlier works, e.g., [5]). That allows us to leverage the message-passing on graph models in the LDPC coded LS-MIMO systems [4], [18]. We also use the uniform scalar quantizer, instead of the non-uniform scalar quantizer. The uniform scalar quantizer is robust to the input distribution, and the maximum quantization error is limited [19].[2] Note that most of the previous works focus on deriving the achievable rate of LS-MIMO channels with low-resolution ADCs [5]–[9], [20], in which the mutual information approach does not account for practical channel coding and modulation schemes. By contrast, the main focus of this work is on practical LS-MIMO communications systems where the protograph LDPC codes are employed.

### C. CONTRIBUTIONS

We aim to develop an analytical tool to investigate the impact of the low-resolution ADCs as well as to provide the engineering insights for the protograph LDPC code design and evaluation in LS-MIMO systems. Our major contributions are summarized as follows:

- Adopting the additive quantization noise model (AQNM) model, we propose the protograph LDPC coded communications over LS-MIMO channels with low-resolution ADCs in the RF module and the joint detection and decoding in the baseband signal processing module.
- Using the Gaussian approximation approach, we derive the extrinsic information expression of the belief-propagation detector, in which the quantization noise effect and the residual interference noise are taken into account.
- We analyze the extrinsic information functions and propose a new PEXIT algorithm, which is a powerful tool to analyze the asymptotic performance of protograph LDPC codes in LS-MIMO channel with low-resolution ADCs.
- We employ the proposed PEXIT algorithm to evaluate the performance of both punctured and non-punctured protograph LDPC codes under various input parameters including the ADC resolution, the LS-MIMO configuration, the maximum number of iterations, and the code rate.
- We carry out extensive Monte-Carlo simulations to validate the proposed PEXIT algorithm. We found that the performance curves of 3-bit and 4-bit ADC systems

---

[2]The framework in this paper can be extended to the non-uniform scalar quantizer straightforwardly.
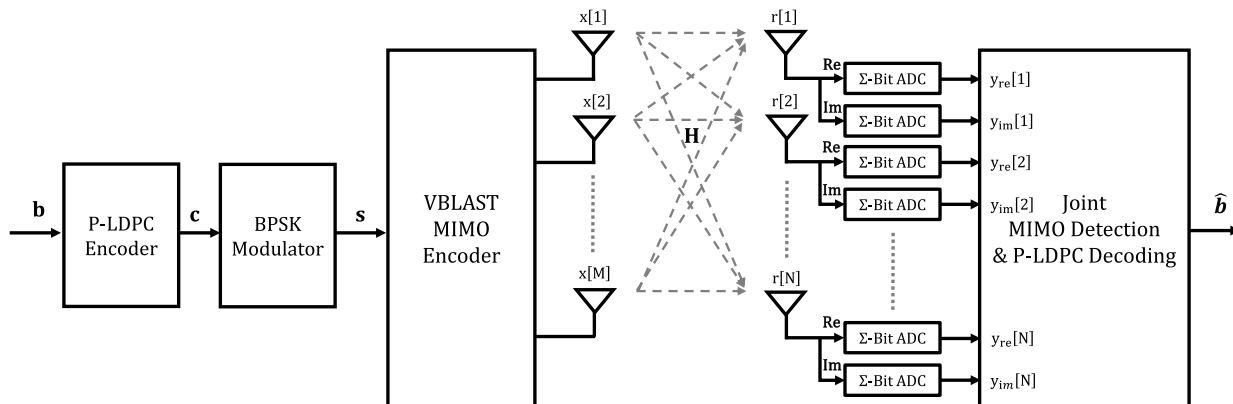
**FIGURE 1.** The channel model of the LS-MIMO coded communication.

have small gaps to that of the high-resolution system. Especially when 5-bit ADC is used, the performance loss is negligible.

### D. OUTLINE

The rest of this paper is organized as follow: Section II presents the LS-MIMO channel model. The joint detection and decoding receiver with soft interference cancellation technique is presented in Section III. In Section IV, we propose a new version of the PEXIT algorithm, which is employed to study the impact of the low-resolution ADCs on the performance of the LS-MIMO communication systems using protograph LDPC codes. In Section V, we apply the proposed PEXIT algorithm to study the performance of LS-MIMO communication systems under various input parameters including the LS-MIMO configuration, the code rate, the number of iterations and the code structure. Section VII concludes the paper.

### II. CHANNEL MODEL

Consider a wireless fading multiple-input-multiple-output (MIMO) channel with $M$ transmitting and $N$ receiving antennas with low-resolution ADCs, as shown in Fig. 1. A block of $K_c$ information bits is first encoded by a P-LPDC encoder that produces a codeword with a length of $N_c$ coded bits. The coded bits $c \in \{0, 1\}$ are passed to a binary-phase-shift-keying (BPSK) modulator whose output is given by $s = (-1)^c \in \{+1, -1\}$. In one channel use, using the spatial multiplexing scheme [21], $M$ modulated symbols are transmitted over $M$ transmitting antennas. It thus requires $L = \lceil N_c/M \rceil$ channel uses to transfer all $N_c$ coded bits.

The received signal model is given by

$$\mathbf{r} = \mathbf{Hx} + \mathbf{w}. \tag{1}$$

Here, $\mathbf{x} = [x[1], x[2], \cdots, x[M]]^T$ is the transmitted symbol whose elements belong to the BPSK modulation alphabet. The average symbol energy $E_s = \mathbb{E}(\|\mathbf{x}\|^2)$ is normalized to 1. $\mathbf{H} \in \mathbb{C}^{N \times M}$ is channel matrix whose entries $h[n, m]$ in the $n$-th row and $m$-th column of $\mathbf{H}$ are modeled as i.i.d complex
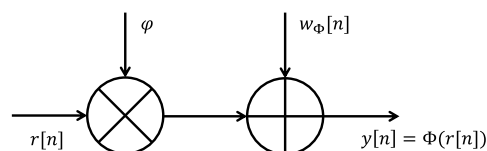
Gaussian with zero mean and unit variance $\mathcal{CN}(0, 1)$. In this work, the perfect channel state information (CSI) is assumed to be available at the receiver, but not at the transmitter. The vector $\mathbf{w} = [w[1], w[2], \cdots, w[N]]^T \in \mathbb{C}^{N \times 1}$ is complex additive white Gaussian noise vector whose entries obey i.i.d complex Gaussian with zero mean and $N_0$ variance (i.e., $\mathcal{CN}(0, N_0)$). Finally, $\mathbf{r} = [r[1], r[2], \cdots, r[N]]^T \in \mathbb{C}^{N \times 1}$ is the received signal vector whose element $r[n]$ is the received signal at the $n$-th antenna.

The received signal at each receive antenna is first converted from the analog form to the digital form by a pair of low-resolution $\Sigma$-bit ADCs: One $\Sigma$-bit ADC is for the in-phase (real) component of the signal and the other $\Sigma$-bit ADC is for the quadrature (imaginary) component of the signal. Let $\Phi$ be the quantization operator, the relation between the input and output of the $\Sigma$-bit ADC block is given by

$$\mathbf{y} = \Phi(\mathbf{r}_{re}) + j\Phi(\mathbf{r}_{im}), \tag{2}$$

where $\mathbf{r}_{re}$ and $\mathbf{r}_{im}$ are the real and imaginary components of the received signal $\mathbf{r}$, respectively. Furthermore, the quantizer $\Phi$ is the scalar one (i.e., each element in the vector is quantized separately).

In this paper, adopting the additive quantization noise model (AQNM) in MIMO systems with low-resolution ADCs [5], [7], we consider the quantization noise as the additive noise component to the input signal. According to the AQNM model in Fig. 2, the relationship between the input and output of the quantizer in (2) can be written as below [5]

$$\mathbf{y} = \varphi \mathbf{r} + \mathbf{w}_\Phi, \tag{3}$$

where $\varphi = 1 - \rho$ and $\rho$ is the inverse of the signal-to-quantization-noise ratio. $\mathbf{w}_\Phi$ is the additive Gaussian noise



**FIGURE 2.** Additive quantization noise model.

vector that is assumed uncorrelatd with **r**. For a given channel realization matrix **H**, the variance of $w_\Phi[n]$, $n = 1, 2, \cdots, N$ is given by [5]

$$\sigma^2_{w_\Phi[n]} = \varphi(1 - \varphi) \left( \sum_{m=1}^{M} |h[n, m]|^2 + N_0 \right), \qquad (4)$$

which depends on the fading channel gains $h[n, m]$ and the additive Gaussian noise at the receiver antenna. Here $N_0$ is again the variance of the additive Gaussian noise in (1).

Here we assume uniform quantizers [22] but our following analysis is also applicable to non-uniform ones. With the assumption of the channel model in (1), the input signals of the $\Sigma$-bit ADCs in Fig. 1 are continuous random variables with infinite support. Therefore, the input signal, $r[n]$, is first truncated to have the finite support in the range $[-L_s, L_s]$ as below:

$$\overline{r[n]} = \begin{cases} -L_s, & r[n] < -L_s; \\ r[n], & -L_s \le r[n] \le L_s; \\ L_s, & r[n] > L_s. \end{cases} \qquad (5)$$

where $\overline{r[n]}$ be the truncated version of the received signal $r[n]$. Generally, the optimal value of $L_s$ depends on the probability density distribution of the input signal and the number of quantization levels [23]. However, for sake's simplicity, the value of $L_s$ is chosen according to the *three-sigma* rule as in [24] to find the truncation limit for the received signal $r[n]$, $n = 1, 2, \cdots, N$ as below:

$$L_s = 3\sigma_{r[n]} = 3 \times (0.5 + 0.5 \times N_0)^{\frac{1}{2}}. \qquad (6)$$

With the uniform scalar quantizer, the quantization noise power is well approximated as $\frac{\Delta^2}{12}$ [19], [23], where $\Delta = \frac{2L_s}{2^\Sigma}$ is the quantization step and $\Sigma$ is the number of quantization bits used in the ADCs. As a result, the parameter $\varphi$ in (4) is approximated by

$$\varphi = 1 - \frac{3}{2^{2\Sigma}}. \qquad (7)$$

Note that the parameter $\varphi$ depends only on the resolution of the ADCs, not on $L_s$ since we assume that the noise due to truncation is negligible in comparison with the quantization noise. The quantized signal **y** is sent to the joint detection and decoding module to restore the original transmit information bitstream. In the following section, we present the joint detection and decoding module for LS-MIMO communications systems with low-resolution ADCs.

## III. JOINT DETECTION AND DECODING RECEIVER FOR LOW-RESOLUTION ADC LS-MIMO SYSTEMS

When the number of antennas is in order of tens or hundreds, the conventional MIMO detection algorithms such as zero-forcing, minimum mean square error spatial filtering, sphere decoding, and maximum likelihood detector are computationally prohibitive [11], [12]. Alternatively, the message-passing algorithm is an attractive solution to deal with the complexity issue. Nonetheless, the previous message-passing
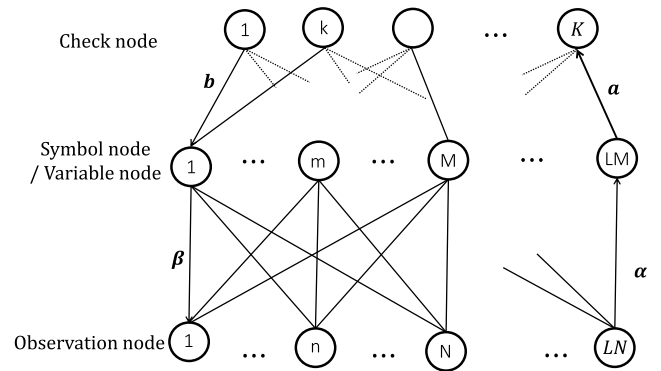


**FIGURE 3.** Double-layer graph for joint detection and decoding receiver.

algorithms are derived for high-resolution LS-MIMO systems. One cannot directly apply these algorithms to the LS-MIMO systems with low-resolution ADCs due to the extra additive quantization noise as well as the change in the amplitude of the input signal given in (3). This section aims to derive a new message-passing algorithm that takes into account the quantization effect of the low-resolution ADCs.

To describe the joint detection and decoding algorithm, we use a double-layer graph, as shown in Fig. 3. The double-layer graph has three types of nodes, namely: 1) $L \times N$ observation nodes representing the received signal sequence **y**; 2) $N_c = L \times M$ symbol nodes that represent the transmit symbol sequence **x**; 3) Finally, there are $K = N_c - K_c$ check nodes that represent the check equations of given P-LDPC codes. The connection of the variable node and the check node is governed by the parity matrix of the LDPC code. In one channel use, the $N$ observation nodes and the $M$ symbol nodes are fully connected to form a graph for the MIMO detection part (i.e., one observation node is connected to all $M$ symbol nodes). In the graph for the LDPC decoding part, there are $N_c$ variable nodes that represent the codeword bit sequence **c**. With the BPSK modulation scheme, the one-one mapping is used to map a codeword bit to a transmit symbol. Therefore, the variable node and the symbol node are merged in a single node on the double-layer graph. Consequently, the two terms, the variable node and symbol node, are used interchangeably in this paper.

In the iterative joint detection and decoding algorithm, there are five types of messages passed over the graph as follows:
- $\alpha[n, m]$ is the message passed from the $n$-th observation node to the $m$-th symbol node.
- $a[m, k]$ is the message passed from the $m$-th variable node to the $k$-th check node.
- $b[k, m]$ is the message passed from the $k$-th check node to the $m$-th variable node.
- $\beta[m, n]$ is the message passing from the $m$-th symbol node to the $n$-th observation node.
- $\Gamma[m]$ is the a posteriori log-likelihood ratio (LLR) value of the symbol $x[m]$.

In the sequel, we describe the operation of the message passing joint detection and decoding receiver with soft symbol cancellation.

## A. MESSAGE PASSED FROM OBSERVATION NODES TO SYMBOL NODES

The received signal at the $n$-th observation node is given as

$$
\begin{aligned}
y[n, m] &= \varphi r[n] + w_\Phi[n] \\
&= \varphi \sum_{m=1}^{M} h[n, m]x[m] + \varphi w[n] + w_\Phi[n] \\
&= \varphi h[n, m]x[m] + \varphi \underbrace{\sum_{t=1, t \neq m}^{M} h[n, t]x[t]}_{Interference} \\
&\quad + \varphi w[n] + w_\Phi[n].
\end{aligned}
\tag{8}
$$

In comparison with the unquantized system (or high-resolution system), the received signal at the $n$-th antenna for the symbol $x[m]$ has one extra noise component (quantization noise), and its signal strength is affected by the quantization process with a factor $\varphi$.

In this paper, the parallel interference cancellation technique [12] is employed to cancel the inter-substream interference in (8). The soft symbol is first estimated based on the extrinsic message passed from the $m$-th symbol node to the $n$-th observation node. Let $\hat{x}[n, m]$ denote the soft symbol obtained from the message passed from the $n$-th observation node to the $n$-th symbol node. For the BPSK modulation scheme,[3] the soft symbol is given by

$$
\hat{x}[n, m] = \tanh\left(\frac{\beta[m, n]}{2}\right),
\tag{9}
$$

where $\beta[m, n]$ is the extrinsic message passed from the $m$-th symbol node to the $n$-th observation node. We assume that $\beta[m, n], \forall n = 1, 2, \cdots, LN, \forall m = 1, 2, \cdots, LM$ are uncorrelated and satisfies the consistency condition [25]. The soft symbol in (9) is now used to cancel the interference from the received signal at the $n$-th observation node for the $m$-th transmit symbol, $x[m]$, as below

$$
\hat{y}[n, m] = y[n, m] - \varphi \sum_{t=1, t \neq m}^{M} h[n, t]\hat{x}[n, t],
\tag{10}
$$

where $\hat{y}[n, m]$ is the received signal of the transmitted symbol $x[m]$ at the $n$-th observation node after the interference cancellation.

Generally, the soft symbol $\hat{x}[n, m]$ is an imperfect replica of the transmitted symbol $x[m]$. Therefore, the residual interference remains in the signal $\hat{y}[n, m]$ after cancellation. Let $z[n, m]$ be the residual interference plus noise components. We have

$$
\begin{aligned}
z[n, m] = \varphi \sum_{t=1, t \neq m}^{M} h[n, t](x[n, t] - \hat{x}[n, t]) \\
+ \varphi w[n] + w_\Phi[n].
\end{aligned}
\tag{11}
$$

[3]It is straightforward to extend to higher-order modulation schemes, as shown in [12].

We can now rewrite $\hat{y}[n, m]$ as below

$$
\hat{y}[n, m] = \varphi h[n, m]x[m] + z[n, m].
\tag{12}
$$

By approximating the residual interference as additive Gaussian noise, the power of the residual interference plus noise components, $z[n, m]$, is calculated as

$$
\begin{aligned}
\Psi[n, m] &= \varphi^2 \sum_{t=1, t \neq m}^{M} |h[n, t]|^2(1 - |\hat{x}[n, t]|^2) \\
&\quad + \varphi^2 N_0 + \varphi(1-\varphi)\left(\sum_{m=1}^{M} |h[n, m]|^2 + N_0\right).
\end{aligned}
\tag{13}
$$

The message passed from the $n$-th observation node to the $m$-th variable node is the log-likelihood ratio (LLR) and given by

$$
\begin{aligned}
\alpha[n, m] &= \ln \frac{\Pr(\hat{y}[n, m]|\mathbf{H}, x[m] = +1)}{\Pr(\hat{y}[n, m]|\mathbf{H}, x[m] = -1)} \\
&= \frac{4\varphi}{\Psi[n, m]}\Re(h^*[n, m]\hat{y}[n, m]).
\end{aligned}
\tag{14}
$$

There are total $N$ messages sent to a given symbol node (or transmit symbol), and the sum of all the messages is equivalent to the channel message (i.e., $L_{ch}$) in the conventional message-passing algorithm [17]. Compared to the expression derived in [11], the new expression in (14) takes into account the quantization noise effect via the parameter $\varphi$ and $\Psi[n, m]$, which depend on the resolution of the ADCs and the fading channels as aforementioned. When the low-resolution ADCs is used, the factor $4\varphi/\Psi[n, m]$ in (14) decreases as $\varphi$ is proportional to the resolution of the ADCs. The channel message, $\alpha[n, m]$ sent to the variable nodes in (14) therefore decreases. Ultimately, the performance of the channel decoder is degraded accordingly. In the high-resolution limit (i.e., $\Sigma \to \infty$) where the parameter $\varphi \to 1$ and the third term of (13) is significantly small, and thus the channel message of the low-resolution ADC approaches that of the high-resolution one in [11]. Our extensive experiments with both analysis and simulation reveal that the performance of the LS-MIMO systems with the 5-bit ADC approaches that of the LS-MIMO system with high-resolution one.

## B. MESSAGE PASSED FROM VARIABLE NODES TO CHECK NODES

Considering the $m$-th variable node, two types of messages are sent to this node. The first type of messages is from the $N$ observation nodes belonging to the part of the MIMO detection graph, and the other type of messages is from the check nodes belonging to the part of the LDPC decoding graph. As a result, the extrinsic message from the $m$-th variable node to the $k$-th check node is the sum of all the messages from the observation nodes and the check nodes except the message from the $k$-th check node. We have

$$
a[m, k] = \sum_{t \in \mathcal{N}_o(m)} \alpha[t, m] + \sum_{t \in \mathcal{N}_c(m) \backslash k} b[t, m],
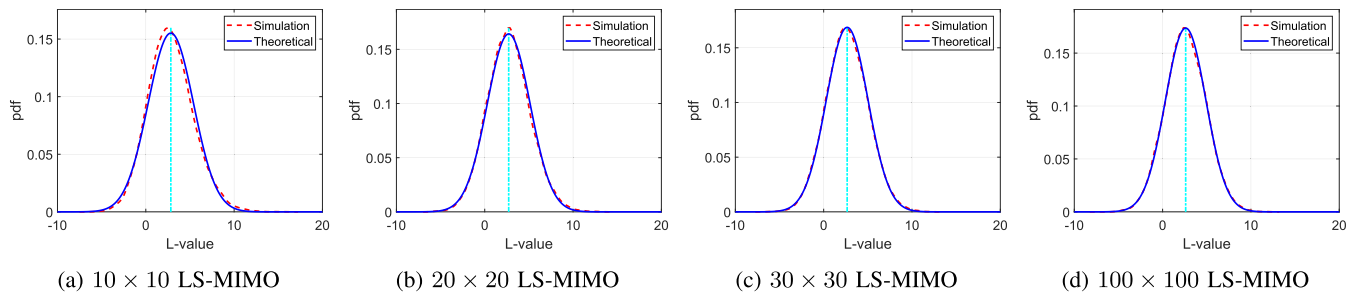\tag{15}
$$

**FIGURE 4.** Pdfs of L-value at the output of the detector: AR3AR code, 5-bit ADC, 10 iterations, code rate $R = 1/2$, blocklength: 9600 bits.

where $\mathcal{N}_c(m)$ is the set of check nodes connected to the $m$-th variable node, and $\mathcal{N}_o(m)$ is the set of observation nodes connected to the $m$-th variable node.

In comparison with the conventional PEXIT, the first term on the right hand side of (15), i.e., $\sum_{t \in \mathcal{N}_o(m)} \alpha[t, m]$, plays the role of the channel LLR message. That the channel LLR message follows the symmetric Gaussian distribution is one of the essential assumptions in the development of the PEXIT algorithm [14]. To justify the Gaussian assumption in this paper, we use a rate-1/2 AR3A code to carry out the Monte Carlo simulations for different MIMO configurations at $SNR = 5.6$ dB. Also, the blocklength and the maximum number of iterations are set to 9600 bits and 10, respectively. Denote the first term as L-value, the probability density functions (pdf) of the $L$-value are plotted in Fig. 4 where the solid curves are for the theoretical results, and the dashed curves are for the simulation results. Note that, Fig. 4 shows the pdfs for the 5-bit ADC only. For the other ADC resolutions, readers are referred to Fig.14 - Fig.17.

The pdf curves indicate that the assumption of Gaussian distribution is generally reasonable for all $10 \times 10$, $20 \times 20$, $30 \times 30$, and $100 \times 100$ MIMO configurations. The biggest discrepancy occurs to the case of the $10 \times 10$ MIMO configuration. However, the difference between the two happens in the small area around the mean of the L-value. Furthermore, this phenomenon happens to all ADC resolutions. In the tail areas, the theoretical and the simulation curves are tight together. The disparity becomes negligible when the number of transmitting antennas increases to 20. In the particular case of 100 transmitting antennas, there is no distinction between the theoretical and simulation curves. As a result, the PEXIT algorithm, proposed in the later section, will be more accurate when the number of transmitting antennas is large.

### C. MESSAGE PASSED FROM CHECK NODES TO VARIABLE NODES

The message from the $k$-th check node to the $m$-th variable node is identical to the conventional message-passing algorithm [17] and given by

$$b[k, m] = \ln \frac{1 - \prod_{t \in \mathcal{N}_v(k) \backslash m} \frac{1 - e^{a[t,k]}}{1 + e^{a[t,k]}}}{1 + \prod_{t \in \mathcal{N}_v(k) \backslash m} \frac{1 - e^{a[t,k]}}{1 + e^{a[t,k]}}}, \quad (16)$$

where $\mathcal{N}_v(k)$ is the set of variable nodes connected to the $k$-th check node. In practical implementation, the computation of $b[k, m]$ is simplified by using the tanh($\cdot$) function.

### D. MESSAGE PASSED FROM SYMBOL NODES TO OBSERVATION NODES

As mentioned above, the $m$-th symbol node receives messages from both the observation nodes and the check nodes. The extrinsic message sent from the $m$-th symbol node to the $n$-th observation node is the sum of all the messages except the message from the $n$-th observation node. As a result, the message from the $m$-th variable node to the $n$-th observation node is given by

$$\beta[m, n] = \sum_{t \in \mathcal{N}_o(m) \backslash n} \alpha[t, m] + \sum_{t \in \mathcal{N}_c(m)} b[t, m], \quad (17)$$

where $\mathcal{N}_o(m)$ and $\mathcal{N}_c(m)$ are the sets of all observation nodes and check nodes that are connected to the $m$-th symbol node, respectively.

### E. A POSTERIORI MESSAGES OF CODEWORD BITS

The posterior LLR of the $m$-th transmit symbol at the end of each iteration is the total messages from both the observation nodes and the check nodes, and it is given by

$$\Gamma[m] = \sum_{n \in \mathcal{N}_o(m)} \alpha[n, m] + \sum_{k \in \mathcal{N}_c(m)} b[k, m]. \quad (18)$$

The posteriori LLR is sent to the hard decision device to produce the decoded version of the codeword bit using the following rule:

$$\hat{c}[m] = \begin{cases} 0, & \Gamma[m] > 0; \\ 1, & \text{Otherwise.} \end{cases} \quad (19)$$

where $\hat{c}[m]$ denotes the decoded version of $c[m]$. And thus, the decoded sequence of the information $\hat{\mathbf{b}}$ is obtained.

The message-passing process stops when all check equations are satisfied, or the maximum number of iterations is reached. Otherwise, the message-passing process repeats with a message update from the observation nodes in Subsection III-A.
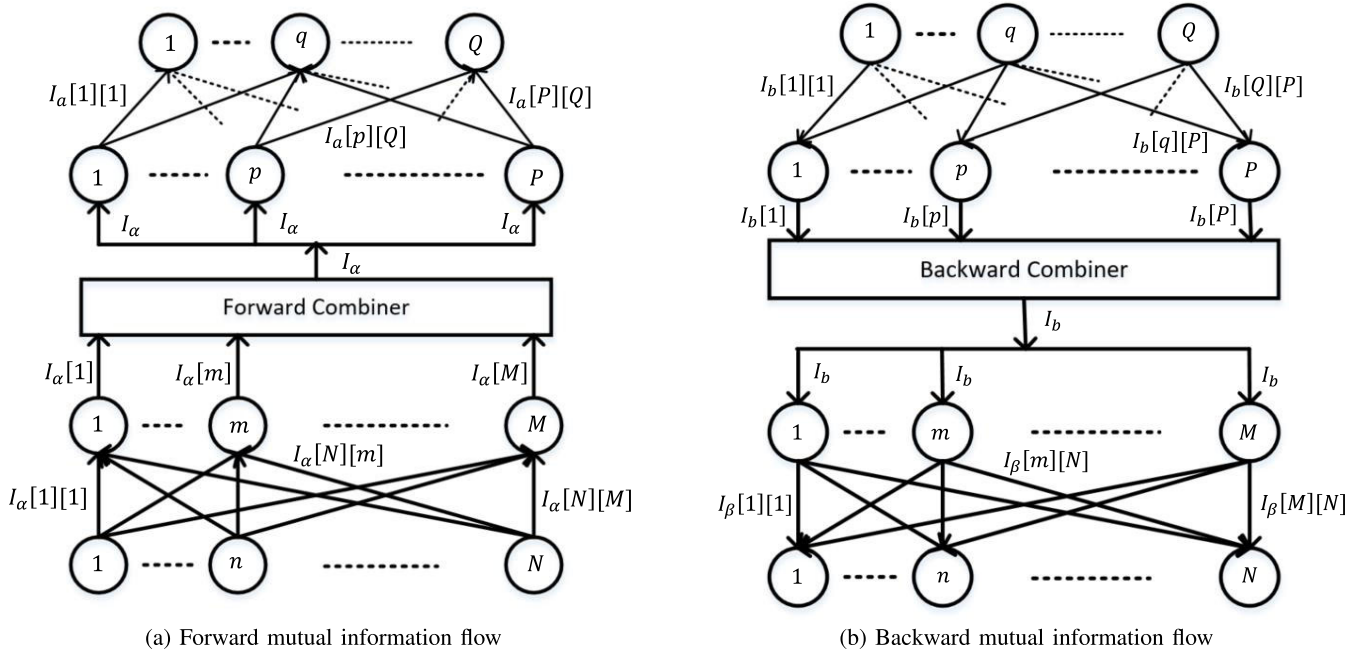
(a) Forward mutual information flow

(b) Backward mutual information flow

**FIGURE 5.** Joint MIMO-LDPC protograph.

## IV. PROPOSED PEXIT ALGORITHM FOR LOW-RESOLUTION ADC LS-MIMO SYSTEMS

The PEXIT algorithm has been widely used as a powerful tool to predict the performance of protograph LDPC codes for various channel models [14], [16]. However, it was designed for high-resolution systems, single-input single-output (SISO) or conventional MIMO systems. In this section, taking into account the impact of the low-resolution ADCs, we propose a new PEXIT algorithm that is suitable for the joint message-passing detection and decoding in LS-MIMO systems.

### A. JOINT MIMO-LDPC PROTOGRAPH

The joint MIMO-LDPC protograph is depicted in Fig. 5. This protograph is a down-scaled version of the double-layer graph in Fig. 3. To facilitate the information flow analysis below, we separate the variable nodes and the symbol nodes into two entities, and they are linked by a forward combiner for the forward information flow and a backward combiner for the backward information flow, respectively.

The MIMO part of the joint MIMO-LDPC protograph has $N$ observation nodes, $M$ symbol nodes, and $M \times N$ edges. This part is duplicated $L$ times to obtain the same MIMO part of the double-layer graph in Fig. 3. Here again, $L$ is the number of channel uses. Whereas, the LDPC part of the joint MIMO-LDPC protograph has $P$ variable nodes, $Q$ check nodes, and a set of edges to connect the variable nodes and check nodes together. The edge connection is defined by a proto-matrix $\mathbf{G}$ of size $Q \times P$. The element $\mathbf{G}[q, p]$ indicates the number of parallel edges that connect the $q$-th check node to the $p$-th variable node. In order to obtain the LDPC part of the double-layer graph in Fig. 3, the LDPC part of the joint MIMO-LDPC protograph is first copied $\delta = \frac{N_c}{P} = \frac{LM}{P}$ times

and then the permutation operation is applied on $\delta$ variable-to-check pairs (edges), corresponding to the same edge type of the original protograph [26]. Note that the number of check nodes $Q = \frac{(N_c - K_c)}{\delta} = (1 - R) \times P$.

We define 5 main types of mutual information, corresponding to the 5 messages on the double-layer graph in Fig. 3, on the joint MIMO and LDPC protograph, as follows:

1) $I_\alpha[n, m]$ is the extrinsic mutual information between the LLR value $\alpha[n, m]$ sent by the $n$-th observation node to the $m$-th variable node and the $m$-th corresponding coded bit.
2) $I_a[p, q]$ is the extrinsic mutual information between the LLR value $a[p, q]$ sent by the $p$-th variable node to the $q$-th check node and the $p$-th corresponding coded bit.
3) $I_b[q, p]$ is the extrinsic mutual information between the LLR value $b[q, p]$ sent by the $q$-th check node to the $p$-th variable node and the $p$-th corresponding coded bit.
4) $I_\beta[m, n]$ is the extrinsic mutual information between the LLR value $\beta[m, n]$ sent by the $m$-th symbol node to the $n$-th observation node and the $m$-th corresponding symbol.
5) $I_\Gamma[p]$ is the posteriori mutual information between the a posteriori LLR value $\Gamma[p]$ and the corresponding code-word bit of the $p$-th variable node.

Besides, we denote the punctured label $P_p$ of the $p$-th variable node as 0 if the $p$-th variable node is punctured (i.e., the codeword bits corresponding to this variable node are not transmitted) and 1 otherwise.

### B. FORWARD MUTUAL INFORMATION FLOW

The forward mutual information flow is the direction in which the extrinsic mutual information flows from the observation

nodes, goes through the symbol nodes and the variable nodes, and ends at the check nodes as shown in Fig. 5a. In the following, the mutual information functions that flow in the forward direction are analyzed.

### 1) MUTUAL INFORMATION $I_\alpha[n, m]$

The $m$-th symbol node receives $N$ LLR values sent from all $N$ observation nodes due to the broadcast nature of the radio signal in LS-MIMO channels. For a fixed channel realization matrix $\mathbf{H}$, the LLR messages transferred from the $n$-th observation node to the $m$-th variable node, $\alpha[n, m]$ derived in (14), is given

$$
\begin{aligned}
\alpha[n, m] &= \frac{4\varphi}{\Psi[n, m]} \Re(h^*[n, m]\hat{y}[n, m]) \\
&= \frac{4}{\Psi[n, m]} \Re(\varphi^2|(h[n, m]|^2 x[m] + \varphi z[n, m])) \\
&= \frac{4}{\Psi[n, m]} (\varphi^2|h[n, m]|^2 x[m] + \varphi\Re(h^*[n, m]z[n, m])).
\end{aligned}
$$

(20)

Without loss of generality, we assume that the all-zero codeword is transmitted. And thus, the LLR value $\alpha[n, m]$ is given by

$$
\alpha[n, m] = \frac{4}{\Psi[n, m]} (\varphi^2|h[n, m]|^2 + \varphi\Re(h^*[n, m]z[n, m])).
$$

(21)

Since $\mathbb{E}[z[n, m]z^*[n, m]] = \Psi[n, m]$ with $\mathbb{E}(\cdot)$ is expectation operator, we have

$$
\begin{aligned}
&\left(\varphi^2|h[n, m]|^2 + \varphi\Re(h^*[n, m]z[n, m])\right) \\
&\sim \mathcal{N}\left(\varphi^2|h[n, m]|^2, \frac{\varphi^2|h[n, m]|^2\Psi[n, m]}{2}\right).
\end{aligned}
$$

(22)

Consequently, we have

$$
\alpha[n, m] \sim \mathcal{N}\left(\frac{\sigma_\alpha^2[n, m]}{2}, \sigma_\alpha^2[n, m]\right),
$$

(23)

with

$$
\sigma_\alpha^2[n, m] = \frac{8\varphi^2|h[n, m]|^2}{\Psi[n, m]}.
$$

(24)

The LLR $\alpha[n, m]$ satisfies the symmetric Gaussian distribution for a given channel realization [16]. We achieve the result in (23) with assumption that the interference plus noise components $z[n, m]$ is approximated i.i.d complex Gaussian random variable. For the high-resolution case, it was verified by both EXIT chart analysis and simulation result that this assumption is reasonable when the number of receive antenna is large [27].

### 2) MUTUAL INFORMATION FROM SYMBOL NODES TO VARIABLE NODES

The $m$-th symbol node receives total $M$ messages from the $M$ observation nodes. Let $\alpha[m]$ be the total message that the $m$th

symbol node receives, we have

$$
\alpha[m] = \sum_{n=1}^{N} \alpha[n, m].
$$

(25)

According to (23), the total message also follows the Gaussian distribution with mean and variance as follows:

$$
\alpha[m] \sim \mathcal{N}(\frac{\sigma_\alpha^2[m]}{2}, \sigma_\alpha^2[m]),
$$

(26)

where

$$
\sigma_\alpha^2[m] = \sum_{n=1}^{N} \sigma_\alpha^2[n, m] = \sum_{n=1}^{N} \frac{8\varphi^2|h[n, m]|^2}{\Psi[n, m]},
$$

(27)

and thus the extrinsic mutual information, $I_\alpha[m]$, is obtained by the following equation

$$
I_\alpha[m] = J(\sigma_\alpha[m])
$$

(28)

with $J(x)$ is given in [17].

Note that the $I_\alpha[m]$ plays the same role as the channel mutual information $I_{ch}$, coupled from the channel to the variable node, in the conventional PEXIT algorithm [14]. We interpret $I_\alpha[m]$ as a generic version of $I_{ch}$ where both the residual interference and the quantization noise effect are taken into account. In the case of the high-resolution limit of the ADCs and the perfect interference cancellation, the expression of $I_\alpha[m]$ is identical to that of $I_{ch}$.

Let us discuss the impact of the low-resolution ADCs on the extrinsic mutual information. From (28) and (27), we observe that the resolution of the ADCs influences on the extrinsic mutual information with factor of $\varphi^2/\Psi[n, m]$. As the resolution decreases, the mutual information $I_\alpha[m]$ decreases. Consequently, the required minimum channel signal to noise ratio (SNR) is thus higher to make the PEXIT chart converge. By building the connection between the resolution of the ADCs and the mutual information, we can investigate the theoretical performance of difference protograph LDPC codes with various input parameters. Especially, we can use the analytical results to predict the impact of the low-resolution ADCs as well as find out at which ADC resolution we can approach the performance of the high-resolution system.

Under the assumption of the infinite code length (i.e., $N_c \to \infty$) the code bits belonging to a particular variable node are transmitted by all transmit antennas/symbol nodes with an equal probability of $1/M$. Therefore, the functionality of the forward combiner is to calculate the average mutual information from all symbol nodes and then send to the variable nodes. Let $I_\alpha$ denote the average mutual information from all symbol nodes, we have

$$
I_\alpha = \frac{1}{M} \sum_{m=1}^{M} I_\alpha[m],
$$

(29)

where $I_\alpha[m]$ is given in (28).

As a result, the channel mutual information flowing from the symbol nodes to the $p$-th variable node is given by

$$I_\alpha[p] = P_p I_\alpha, \quad \forall p = 1, 2, \cdots, P. \qquad (30)$$

### 3) MUTUAL INFORMATION FLOW FROM VARIABLE NODES TO CHECK NODES

The expression for the mutual information transferred from the $p$-th variable node to the $q$-th check node, $I_a[p, q]$, is identical to that of the conventional PEXIT algorithm in [14] and given by

$$I_a[p, q] = J\left(\sqrt{[J^{-1}(I_\alpha[p])]^2 + \sigma_b^2[p]}\right), \qquad (31)$$

where

$$\sigma_b^2[p] = \sum_{t \in \mathcal{N}_c(p) \backslash k} \mathbf{G}[t, p][J^{-1}(I_b[t, p])]^2, \qquad (32)$$

where $J^{-1}(x)$ is given in [17].

In (32), $\mathcal{N}_c(p)$ is the set of check nodes that connect to the $p$-th variable node. It is worth noting that $[J^{-1}(I_\alpha[p])]^2$ in (31) is equivalent to $\sigma_{ch}^2$ in the original version of the PEXIT algorithm for AWGN channels [14] and the modified version for the spatial diversity system in [16]. In [16], the authors illustrated that the channel LLR messages do not follow a symmetric Gaussian distribution in the case of a SIMO Rayleigh fading channel. However, it is not the case for the LS-MIMO systems because each channel LLR message, which is expressed in (27), is a sum of $N$ LLR messages from $N$ observation nodes. As a result, leveraging the law of large number, it is reasonable to assume that channel LLR messages follow a symmetric Gaussian distribution. We verify this fact via the Monte Carlo simulation with results which are shown in Fig. 4 and Fig.14 - Fig.17.

### C. BACKWARD MUTUAL INFORMATION FLOW

The back mutual information flow is the direction in which the extrinsic mutual information flows from the check nodes, goes through the symbol nodes and variable nodes, and ends at the observation nodes as shown in Fig. 5b. In what follows, we present the mutual information functions that flow in the backward direction.

### 1) MUTUAL INFORMATION FLOW FROM CHECK NODES TO VARIABLE NODES

The calculation of the mutual information transferred from the $q$-th check node to the $p$-th variable node is identical to that of the conventional PEXIT algorithm in [14]. We have $I_b[q, p]$

$$I_b[q, p] = 1 - J\left(\sigma_a[q]\right), \qquad (33)$$

where

$$\sigma_a^2[q] = \sum_{t \in \mathcal{N}_v(q) \backslash p} \mathbf{G}[q, t][J^{-1}(1 - I_a[t, q])]^2. \qquad (34)$$

### 2) MUTUAL INFORMATION FLOW FROM VARIABLE NODES TO SYMBOL NODES

Let $I_b[p]$ denote the total mutual information that the $p$-th variable node receives from the check nodes. We can express the total mutual information as below

$$I_b[p] = \sum_{q \in \mathcal{N}_c(p)} I_b[q, p]. \qquad (35)$$

Under the same assumption of the infinite code length, the probability that a symbol node transmits the codeword bit from the $p$-th variable node is $1/(\sum_{p=1}^P P_p)$. Therefore, the functionality of the backward combiner is to calculate the average mutual information over all the variable nodes before sending it to the symbol nodes. The average mutual information from the variable nodes to symbol nodes is given by

$$I_b = \frac{1}{(\sum_{p=1}^P P_p)} \sum_{p=1}^P P_p I_b[p]. \qquad (36)$$

### 3) MUTUAL INFORMATION FROM SYMBOL NODES TO OBSERVATION NODES

The mutual information transferred from the $m$-th symbol node to the $n$-th observation node, $I_\beta[m, n]$, is calculated as

$$I_\beta[m, n] = J\left(\sqrt{\sigma_{\alpha*}^2[m] + \sigma_b^2}\right), \qquad (37)$$

where

$$\sigma_b^2 = [J^{-1}(I_b)]^2 \qquad (38)$$

$$\sigma_{\alpha*}^2[m] = \sum_{t \in \mathcal{N}_o(m) \backslash n} [J^{-1}(I_\alpha[t, m])]^2$$

$$= \sum_{t \in \mathcal{N}_o(m) \backslash n} \sigma_\alpha^2[t, m] = \sum_{t \in \mathcal{N}_o(m) \backslash n} \frac{8\varphi^2 |h[t, m]|^2}{\Psi[t, m]} \qquad (39)$$

### D. THE APP MUTUAL INFORMATION

Calculate $I_\Gamma[p]$ for the $p$-th variable node

$$I_\Gamma[p] = J\left(\sqrt{\sigma_\alpha^2 + \sigma_b^2[p]}\right), \qquad (40)$$

where

$$\sigma_b^2[p] = \sum_{t \in \mathcal{N}_c(p)} \mathbf{G}[t, p][J^{-1}(I_b[t, p])]^2 \qquad (41)$$

### E. PROPOSED PEXIT ALGORITHM

The proposed PEXIT algorithm is obtained by applying the mutual information functions in previous subsections with parameters of a given MIMO configuration, $M \times N$, and the size of proto-matrix $\mathbf{G}$, $Q \times P$, and the channel parameter $E_b/N_0$, and the resolution of the ADCs, $\Sigma$. The LS-MIMO-PEXIT algorithm is described below:

**Step 0: Initialization:**
- Calculate $R = \frac{P-Q}{\sum_{p=1}^{P} P_p}$
- Calculate $N_0 = \frac{M}{R(E_b/N_0)}$
- Calculate $\varphi = 1 - 3 \times 2^{-2\Sigma}$
- Set $I_\beta = 0$
- Generate $F$ LS-MIMO channel realization matrices $H_1, H_2, \cdots, H_F$

**Step 1: Observation to variable update**
- For $f = 1, 2, \cdots, F$
  - For $m = 1, 2, \cdots, M$ and $n = 1, 2, \cdots, N$
    * Calculate $\sigma_\beta = J^{-1}(I_\beta)$
    * Generate $\beta_f[m, n] \sim \mathcal{N}(\pm\frac{\sigma_\beta^2}{2}, \sigma_\beta^2)$
    * Estimate soft information $\hat{x}_f[m, n] = \tanh\left(\frac{\beta_f[m,n]}{2}\right)$
    * Calculate $\Psi_f[n, m]$

$$\Psi_f[n, m]$$
$$= \varphi^2 \sum_{t=1, t \neq m}^{M} |h_f[n, t]|^2 (1 - |\hat{x}_f[t, n]|^2)$$
$$+ \varphi^2 N_0 + \varphi(1 - \varphi) \left( \sum_{m=1}^{M} |h_f[n, m]|^2 + N_0 \right)$$

  - For $m = 1, 2, \cdots, M$
    * Calculate $I_{\alpha,f}[m]$

$$I_{\alpha,f}[m] = J\left( \sqrt{\sum_{n=1}^{N} \frac{8\varphi^2 |h_f[n, m]|^2}{\Psi_f[n, m]}} \right)$$

- Calculate the average of $I_{\alpha,f}$ over all the channel realizations

$$I_\alpha[m] = \frac{1}{F} \sum_{f=1}^{F} I_{\alpha,f}[m], \quad \forall m = 1, 2, \cdots, M.$$

- For $p = 1, 2, \cdots, P$, calculate $I_\alpha[p]$

$$I_\alpha[p] = P_p \left( \frac{1}{M} \sum_{m=1}^{M} I_\alpha[m] \right).$$

Note that if the $p$-th variable node is punctured, then $P_p = 0$.

**Step 2: Variable to check update**
- For $p = 1, 2, \cdots, P$ and $q = 1, 2, \cdots, Q$, calculate $I_a[p, q]$
  - if $\mathbf{G}[p, q] \neq 0$

$$I_a[p, q] = J\left( \sqrt{\sum_{t \in \mathcal{N}_c(p) \backslash q} \mathbf{G}[t, p][J^{-1}(I_b[t, p])]^2 + \sigma_\alpha^2[p]} \right)$$

with

$$\sigma_\alpha[p] = J^{-1}(I_\alpha[p]).$$

  - If $\mathbf{G}[p, q] = 0$, $I_a[p, q] = 0$.

**Step 3: Check to variable update**
- For $q = 1, 2, \cdots, Q$ and $p = 1, 2, \cdots, P$
  - if $\mathbf{G}[q, p] \neq 0$

$$I_b[q, p] = 1 - J\left( \sqrt{\sum_{t \in \mathcal{N}_v(q) \backslash p} \mathbf{G}[q, t][J^{-1}(1 - I_a[t, q])]^2} \right)$$

  - If $\mathbf{G}[q, p] = 0$, $I_b[q, p] = 0$

**Step 4: Symbol to observation update**
- For $f = 1, 2, \cdots, F$
  - For $m = 1, 2, \cdots, M$ and $n = 1, 2, \cdots, N$

$$I_{\beta,f}[m, n] = J\left( \sqrt{\sigma_{\alpha_f^*}^2[m] + \sigma_b^2} \right)$$

with

$$\sigma_{\alpha_f^*}[m] = \sum_{t \in \mathcal{N}_o(m) \backslash n} \frac{8\varphi^2 |h_f[t, m]|^2}{\Psi_f[t, m]}$$

and

$$\sigma_b = J^{-1}(I_b) = J^{-1}\left( \frac{\sum_{p=1}^{P} \sum_{q=1}^{Q} I_b[q, p]}{\sum_{p=1}^{P} P[p]} \right)$$

- For $m = 1, 2, \cdots, M$ and $n = 1, 2, \cdots, N$

$$I_\beta[n, m] = \frac{1}{F} \sum_{f=1}^{F} I_{\beta,f}[n, m]$$

**Step 5: APP-LLR mutual information calculation**
- For $p = 1, 2, \cdots, P$

$$I_\Gamma[p] = J\left( \sqrt{\sigma_\alpha^2[p] + \sum_{q=1}^{Q} \mathbf{G}[q, p][J^{-1}(I_b[q, p])]^2} \right)$$

with

$$\sigma_\alpha[p] = J^{-1}(I_\alpha[p])$$

**Step 6: Repeat Step 1 - Step 6 until** $I_\Gamma[p] = 1$, $\forall p = 1, 2, \cdots, P$.

The proposed PEXIT algorithm converges when the select $E_b/N_0$ is above the threshold. Hence, the threshold $(E_b/N_0)^*$ is the lowest value at which the mutual information between the APP-LLR messages and the corresponding codeword bits converges to 1. As can be seen, the proposed PEXIT algorithm for the low-resolution ADCs differs from the conventional PEXIT algorithm [14] in all steps, except Step 3. Specifically, the impact of the low-resolution ADCs is taken into account (in steps 1 and 4) to calculate the mutual information functions.

In the following section, we exploit the proposed PEXIT algorithm to analyze the performance of the LS-MIMO communication systems with low-resolution ADCs.

## V. ANALYSIS OF PROTOGRAPH CODES

We now use the proposed PEXIT algorithm derived in Section IV-E to analyze the performance of the off-the-shelf protograph LDPC codes for LS-MIMO systems. In particular, we pick four protograph LDPC codes whose proto-matrices are given in (42) - (45).

$$G_{AR3A} = \begin{pmatrix} 1 & 2 & 1 & 0 & 0 \\ 0 & 2 & 1 & 1 & 1 \\ 0 & 1 & 2 & 1 & 1 \end{pmatrix}_{3 \times 5} \quad (42)$$

$$\mathbf{G}_{NND} = \begin{pmatrix} 2 & 1 & 0 & 0 & 0 & 1 & 0 \\ 3 & 0 & 1 & 1 & 1 & 1 & 0 \\ 1 & 0 & 2 & 2 & 1 & 2 & 1 \\ 2 & 0 & 0 & 0 & 0 & 0 & 2 \end{pmatrix}_{4 \times 7} \quad (43)$$

The AR3A code in (42) was previously designed for the AWGN channel [15]. This code not only possesses excellent performance at both waterfall region and the error-floor region in the AWGN channel but also was proven in [16] to outperform other LPDC codes including the (3, 6)-regular code, the irregular LDPC code [28] and the AR4JA code in the Rayleigh-fading channel with spatial diversity. In the same punctured class with the AR3A code, we pick the NND code designed in [13]. The protograph of this code has four check nodes and seven variable nodes. Both the AR3A code and NND code, the variable with the highest degree is punctured to obtain the corresponding code rate of 1/2.

$$\mathbf{G}_{UCHI} = \begin{pmatrix} 3 & 3 & 0 & 0 & 1 & 0 & 0 & 0 \\ 2 & 3 & 0 & 1 & 0 & 1 & 0 & 0 \\ 3 & 2 & 1 & 0 & 0 & 2 & 1 & 1 \\ 0 & 0 & 2 & 2 & 2 & 0 & 2 & 1 \end{pmatrix}_{4 \times 8} \quad (44)$$

$$\mathbf{G}_{NTH} = \begin{pmatrix} 3 & 3 & 1 & 0 & 0 & 0 & 0 & 1 \\ 3 & 2 & 0 & 0 & 1 & 0 & 1 & 0 \\ 3 & 1 & 0 & 1 & 2 & 1 & 0 & 0 \\ 3 & 0 & 2 & 2 & 0 & 1 & 1 & 1 \end{pmatrix}_{4 \times 8} \quad (45)$$

In the non-punctured family, we pick two codes, so-called UCHI code [29] and NTH code [26] whose proto-matrices are given in (44) and (45), respectively. The graphs of both UCHI code and NTH code have four check nodes and eight variable nodes. Moreover, they both have a code rate of 1/2.

In this research work, we limit the resolution of the ADCs from 2 to 5 bits. The reason we do not include the 1-bit ADC, which was extensively used [8], [30], is that 1-bit ADC outputs only the sign of the input signal, not the amplitude. Accordingly, it requires special treatment to calculate the soft-output in the message-passing algorithm [8], and we will investigate 1-bit ADC in a separate work.

Employing the proposed PEXIT algorithm, we obtain the iterative decoding thresholds for those four selected codes with different ADC resolutions and LS-MIMO configurations. Particularly, Table 1 and Table 2 present the analytical results for $10 \times 10$ LS-MIMO and $100 \times 100$ LS-MIMO channels, respectively. Here, we use a small number of iterations that is suitable for low-delay and low complexity systems. Results with higher iterations are also reported below.

**TABLE 1.** Iterative decoding threshold: 10 × 10 MIMO, 10 iterations, code rate of 1/2.

| | NND code | AR3A code | UCHI code | NTH code |
|---|---|---|---|---|
| 2-bit ADC | 4.83 | 4.03 | 3.62 | 3.41 |
| 3-bit ADC | 4.11 | 3.40 | 3.04 | 2.86 |
| 4-bit ADC | 3.95 | 3.26 | 2.90 | 2.74 |
| 5-bit ADC | 3.91 | 3.22 | 2.87 | 2.70 |
| Unquantized | 3.91 | 3.22 | 2.86 | 2.70 |

**TABLE 2.** Iterative decoding threshold: 100 × 100 MIMO, 10 iterations, code rate of 1/2.

| | NND code | AR3A code | UCHI code | NTH code |
|---|---|---|---|---|
| 2-bit ADC | 4.59 | 3.84 | 3.46 | 3.29 |
| 3-bit ADC | 3.95 | 3.29 | 2.94 | 2.79 |
| 4-bit ADC | 3.80 | 3.16 | 2.82 | 2.68 |
| 5-bit ADC | 3.77 | 3.13 | 2.79 | 2.65 |
| Unquantized | 3.76 | 3.12 | 2.79 | 2.64 |

**TABLE 3.** Relation between Σ and φ.

| Σ | 2 | 3 | 4 | 5 | 12 (high-resolution) |
|---|---|---|---|---|---|
| φ | 0.8125 | 0.9531 | 0.9883 | 0.9971 | 0.9999 |

The iterative decoding threshold results indicate that the NND code has poorer performance than the AR3A code in all test cases of the ADC resolution. Note that the iterative decoding threshold is the minimum required channel SNR such that the decoder decodes the noisy signal with an arbitrarily small error. Therefore, the lower the iterative decoding threshold, the better the P-LDPC code is. At the 2-bit ADC resolution, the threshold gaps between the AR3A code and the NND code are 0.8 dB for $10 \times 10$ LS-MIMO configuration and 0.75 dB for $100 \times 100$ LS-MIMO configuration, respectively. At the 5-bit ADC resolution, the gaps are slightly reduced to 0.69 dB and 0.64 dB. Based on the formula of complexity level,[4] the complexity of the NND code is 16.67% higher than that of the AR3A code. This fact hints that if one chooses the NND code for LS-MIMO channels with low-resolution ADC over the AR3A code without performance analysis, the decision will lead to not only the high complexity but also the performance loss- in comparison with the AR3A code.

When we fix a P-LDPC code and vary the resolution levels, for example, looking at the NND code in Table 1, one can see that changing from the 2-bit ADC resolution to the 3-bit ADC resolution can improve the iterative decoding threshold of about 0.72 dB. The gain of the iterative decoding threshold in changing the resolution level from the 3-bit ADC to the 4-bit ADC is 0.16 dB. Moreover, the iterative decoding threshold gap between the 5-bit ADC and the unquantized (or high-resolution) is at most 0.01 dB. This very tiny gap between the 5-bit ADC case and the unquantized case suggests that the 5-bit ADC should be the maximum resolution one should use in the LS-MIMO communication systems while the penalty for the performance is negligible.

---

[4]The complexity level of an iterative decoder for a protograph code is approximately expressed as the product of the number of decoding iterations and the number of edges on the graph [31]

**TABLE 4.** Iterative decoding threshold: 10 × 10 MIMO configuration, AR3A code with code rate of 1/2, 10 − 50 iterations.

|            | 5-Ite. | 10-Ite. | 15-Ite. | 20-Ite. | 50-Ite. |
|------------|--------|---------|---------|---------|---------|
| 2-bit ADC  | 6.82   | 4.03    | 3.12    | 2.68    | 2.02    |
| 3-bit ADC  | 5.74   | 3.40    | 2.61    | 2.23    | 1.64    |
| 4-bit ADC  | 5.49   | 3.26    | 2.49    | 2.11    | 1.55    |
| 5-bit ADC  | 5.44   | 3.22    | 2.46    | 2.09    | 1.53    |
| Unquantized| 5.42   | 3.22    | 2.45    | 2.09    | 1.53    |

Lowering the ADC resolution to 3-bit or 4-bit leads to a bigger performance gap compared with the high-resolution one. For example, looking at the AR3A code, the threshold gaps are 0.18 dB and 0.04 dB for the 3-bit ADC and the 4-bit ADC, respectively. The same conclusion is applied to the other three codes as well as 100 × 100 LS-MIMO channels. Let us look at the analytical expressions in (13) and (14) to understand this phenomenon deeply. At the 5-bit resolution, the value of the parameter $\varphi$ is very close to that of the high-resolution (see Table 3) and approaches 1. Consequently, the third term in (13) is significantly small in comparison with the residual interference plus Gaussian noise component. Ultimately, the impact of the quantization process vanishes. In the same token, we can also observe the behavior of the 3-bit and 4-bit ADCs.

Now, we fix the LS-MIMO configuration to 10 × 10 and the AR3A code with a code rate of 1/2, and we vary the number of iterations. The iterative decoding thresholds of the AR3A code are given in Table 4. Examining the performance improvement when changing from 5 iterations to 10 iterations, one can see that the threshold gap is 2.79 dB and 2 dB at the 2-bit ADC resolution and the 5-bit ADC resolution, respectively. It means that if we double the complexity level, the iterative threshold is improved at about 2 dB. Nevertheless, the gain tends to decline when increasing the number of iterations further. For example, at the 2-bit ADC resolution, if increasing from 10 iterations to 20 iterations, the threshold gap is just 1.35 dB. The gap is smaller when the number of iterations increases. This suggests that the performance gain is diminished when increasing the number of iterations. It is interesting to observe that at any number of iterations, the maximum threshold gaps of the 3-bit ADC and 4-bit ADC resolutions are 0.32 dB and 0.07 dB, respectively. This indicates that the performance loss of using the 3-bit or 4-bit ADC resolution is within the acceptable level. In the 5-bit ADC resolution, the maximum threshold gap, happening at 5 iterations, is 0.02 dB. We, therefore, expect performance of 5-bit ADC approaches that of the unquantized one.

We now look at the thresholds of the AR3A code with a code rate of 1/2 and 10 iterations, as shown in Table 5. As we see, the thresholds decrease as the number of receive antennas increases. Special attention should be given to the scenarios when the number of receiving antennas is from 30 and above. In these scenarios, the thresholds of 3-bit and 4-bit ADCs are very close to the threshold of the unquantized case. Therefore, we expect that we can have a very tight performance gap between 4-bit ADC and unquantized case.

With the help of the modified PEXIT algorithm, we can also investigate the performance of the protograph LDPC code when the code rate varies. Table 6 shows the iterative decoding thresholds of AR3A family with the code rate ranging from 1/2 to 9/10. The gap between the 2-bit ADC and the 3-bit ADC increases when the code rate increases. For example, at the code rate of 1/2, the gap between the 2-bit ADC and the 3-bit ADC is 0.63 dB. Whereas, the gap between those two corresponding ADC resolutions is 2.93 dB at the code rate of 9/10. It is also that the gap between the 5-bit ADC and the unquantized is at most 0.03 dB (at high code rate). As a result, we expect to have a tiny performance gap between the 5-bit ADC system and the unquantized one.

With the analysis of iterative decoding thresholds of the protograph LDPC codes in various input parameters, we can close this section with a conclusion that the 3-bit ADC and 4-bit ADC has small threshold gaps to the unquantized one and the 5-bit ADC can approach the performance of the unquantized one for LS-MIMO channels. The small iterative decoding threshold gaps are translated to the slight differences in the bit error rate (BER) curves. This fact will be verified in Section VI.

## VI. SIMULATION RESULTS

In Section V, we have represented the analytical results of protograph LDPC codes with a variety of operation scenarios. In the following, we report simulation results to validate the analytic results and provide insights on the impact of the low-resolution ADCs on the performance of LS-MIMO communications systems.

A protograph LDPC code (or an equivalent LDPC code) is constructed by copy-and-permutation operation on a protograph, a process known as *protograph lifting*. Our protograph codes are derived from protographs in two lifting steps. First, the protograph is lifted by a factor of 4 using the progressive edge growth (PEG) algorithm [32] to remove all multiple parallel edges. Then, the second lifting factor is chosen to match the required code block length. For example, the AR3A code with the proto-matrix size of 3 × 5 and rate of 1/2, the second lifting factor is 600 to achieve the ultimate code block length of 9600 bits. The PEG algorithm was applied to determine a circulant permutation of each edge class to avoid short-length cycles. The decoder is a standard message-passing decoder, in which the maximum number of iterations is set to 10 in all scenarios except the one that we explore the impact of iterations on the performance of LS-MIMO communications systems. LLR clipping and other decoding parameters are set according to [33].

The simulation results in Fig. 6 - Fig. 9 verify the analytical results in Table 1 and Table 2. We observe that the simulation results are in good agreement with the analytical results in Section V. In particular, as analyzed above, the NND code has the worst performance among the four selected codes at all the ADC resolution levels. Also, the performance gap between the NND code and the AR3A code is biggest. The small iterative decoding thresholds of the UCHI code and

**TABLE 5.** Iterative decoding threshold: AR3A Code, code rate of 1/2, 10 iterations, $10 \times 10 - 10 \times 80$ LS-MIMO configurations.

| | $10 \times 10$ | $10 \times 20$ | $10 \times 30$ | $10 \times 40$ | $10 \times 50$ | $10 \times 60$ | $10 \times 70$ | $10 \times 80$ |
|---|---|---|---|---|---|---|---|---|
| 2-bit ADC | 4.03 | 0.01 | $-2.03$ | $-3.40$ | $-4.44$ | $-5.27$ | $-5.96$ | $-6.55$ |
| 3-bit ADC | 3.40 | $-0.25$ | $-2.20$ | $-3.53$ | $-4.54$ | $-5.35$ | $-6.03$ | $-6.61$ |
| 4-bit ADC | 3.26 | $-0.31$ | $-2.24$ | $-3.56$ | $-4.56$ | $-5.37$ | $-6.05$ | $-6.63$ |
| 5-bit ADC | 3.22 | $-0.33$ | $-2.25$ | $-3.57$ | $-4.57$ | $-5.38$ | $-6.05$ | $-6.63$ |
| Unquantized | 3.22 | $-0.33$ | $-2.25$ | $-3.57$ | $-4.57$ | $-5.38$ | $-6.05$ | $-6.63$ |

**TABLE 6.** Iterative decoding threshold: AR3A Code, $10 \times 10$ LS-MIMO, 10 iterations, code rate from 1/2 to 9/10.

| | 1/2 | 2/3 | 3/4 | 4/5 | 5/6 | 6/7 | 7/8 | 8/9 | 9/10 |
|---|---|---|---|---|---|---|---|---|---|
| 2-bit ADC | 4.03 | 5.06 | 5.92 | 6.63 | 7.22 | 7.76 | 8.22 | 8.64 | 9.04 |
| 3-bit ADC | 3.40 | 4.02 | 4.53 | 4.93 | 5.24 | 5.51 | 5.74 | 5.94 | 6.11 |
| 4-bit ADC | 3.26 | 3.79 | 4.23 | 4.58 | 4.86 | 5.08 | 5.27 | 5.45 | 5.60 |
| 5-bit ADC | 3.22 | 3.74 | 4.16 | 4.49 | 4.76 | 4.98 | 5.17 | 5.33 | 5.47 |
| Unquantized | 3.22 | 3.72 | 4.14 | 4.47 | 4.74 | 4.95 | 5.14 | 5.30 | 5.44 |



(a) 2-bit ADC    (b) 3-bit ADC    (c) 4-bit ADC    (d) 5-bit ADC + Unquantized
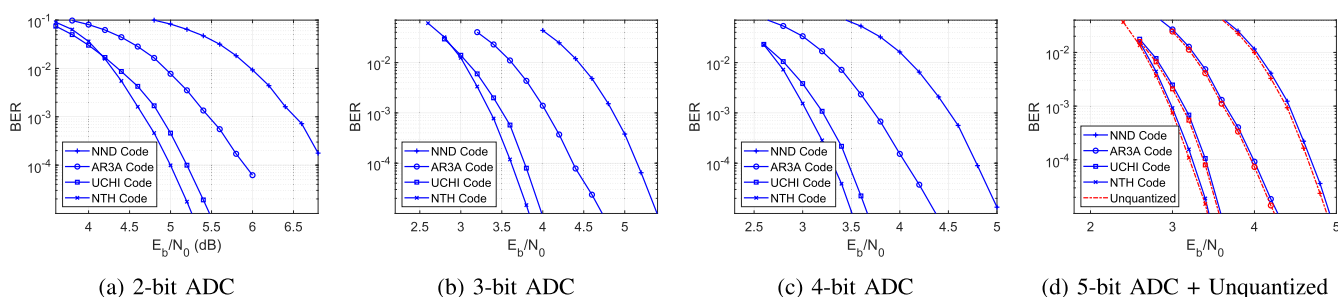
**FIGURE 6.** Comparison BER: $10 \times 10$ MIMO, 10 iterations, code rate $R = 1/2$, blocklength: 9600 bits.



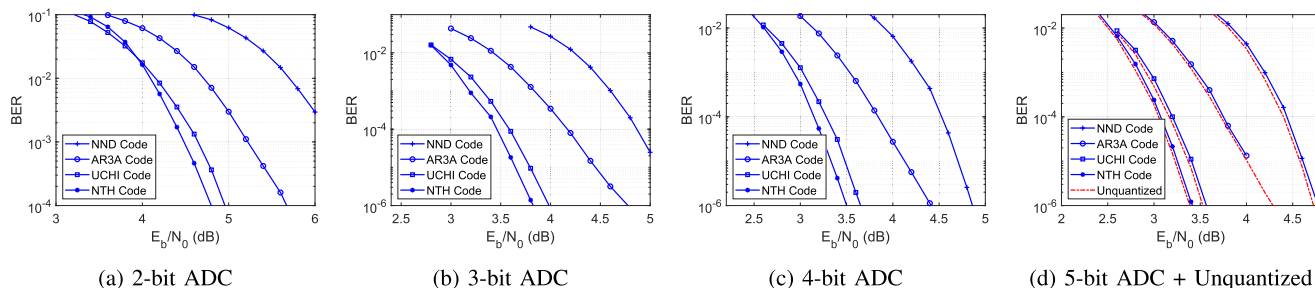(a) 2-bit ADC    (b) 3-bit ADC    (c) 4-bit ADC    (d) 5-bit ADC + Unquantized

**FIGURE 7.** Comparison BER: $100 \times 100$ MIMO, 10 iterations, code rate $R = 1/2$, blocklength: 9600 bits.

the NTH code is interpreted as a small gap in BER curves, as shown in Fig. 6 and Fig. 7.

There is a very tiny difference in iterative decoding thresholds of 5-bit ADC and unquantized one as shown in Table 1 and Table 2. The simulation results validate this analytical result. We see that BER curves of all four codes at the 5-bit ADC and the unquantized one are very tight in both $10 \times 10$ and $100 \times 100$ LS-MIMO configurations.

Consider the performance of a single code in Fig. 8 and Fig. 9, we see that the performance gap between the 2-bit ADC and the 3-bit ADC is around 1.4 dB which is larger than the iterative decoding threshold gap, about 0.8 dB, obtained by the modified PEXIT algorithm. This phenomenon is well-known for the PEXIT algorithm due to the Gaussian approximation in the LLR messages [14]. However, the analytical results can predict exactly performance trends of the code under the various ADC resolution levels. Let us take a closer

look at the BER curves of the AR3A code in Fig. 8 and Fig. 9, the BER gap of the 3-bit ADC and the unquantized one is about 0.4 dB (the threshold gap is 0.18 dB) and the BER gap of the 4-bit ADC and the unquantized one is about 0.1 dB (the threshold gap is 0.04 dB). Similar observations are seen for the other selected codes. These simulation results verify the analytical results that a small performance loss occurs at the 3-bit and 4-bit ADC resolutions in LS-MIMO channels.

The modified PEXIT algorithm can give accurate predict performance of protograph codes in other operation scenarios, including the LS-MIMO configuration and the code rate. For instance, the iterative decoding thresholds, as shown in Table 6, can predict that there is a tiny performance difference between 5-bit ADC system and unquantized system. The simulation results show that the curves of 5-bit ADC systems approach the curves of the unquantized systems in all code rate from 1/2 to 8/9. The accurate performance prediction of
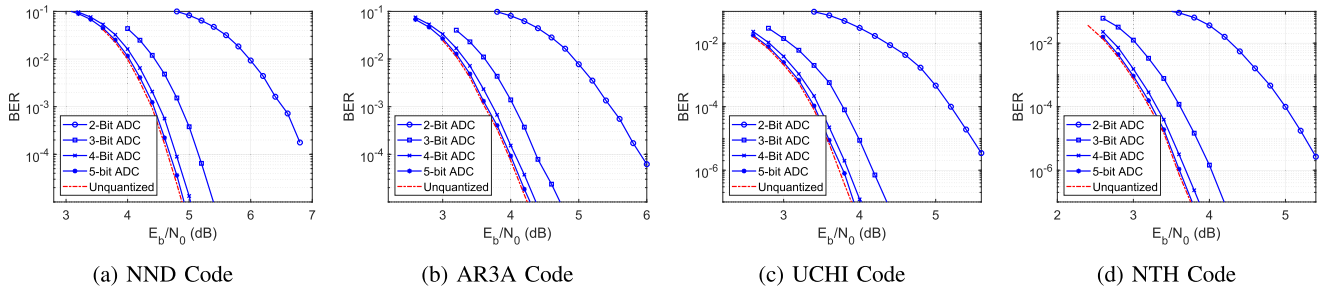
(a) NND Code      (b) AR3A Code      (c) UCHI Code      (d) NTH Code

**FIGURE 8.** BER performance vs. Σ-Bit ADC: 10 × 10 MIMO, 10 iterations, code rate $R = 1/2$, blocklength: 9600 bits.



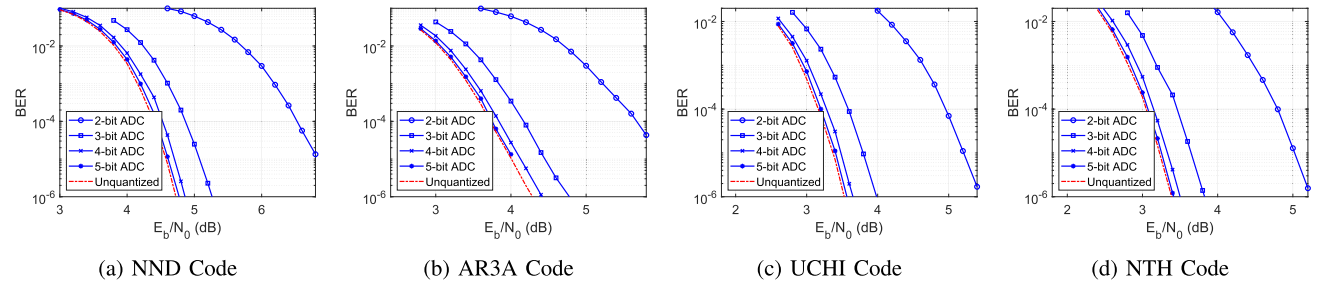(a) NND Code      (b) AR3A Code      (c) UCHI Code      (d) NTH Code

**FIGURE 9.** BER performance vs. Σ-Bit ADC: 100 × 100 MIMO, 10 iterations, code rate $R = 1/2$, blocklength: 9600 bits.
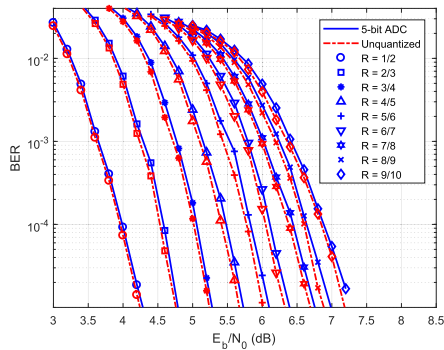


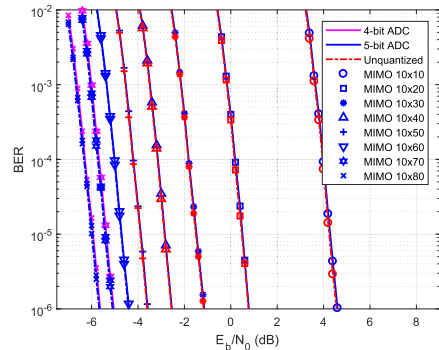**FIGURE 10.** BER vs. code rate: AR3A Code, 10 × 10 MIMO, 10 iterations, code rate $R = 1/2 - 9/10$, block length: 9600 bits.



**FIGURE 12.** BER vs. MIMO configuration: AR3A Code, 10 × 10 MIMO, 10 iterations, code rate $R = 1/2$, block length: 9600 bits.
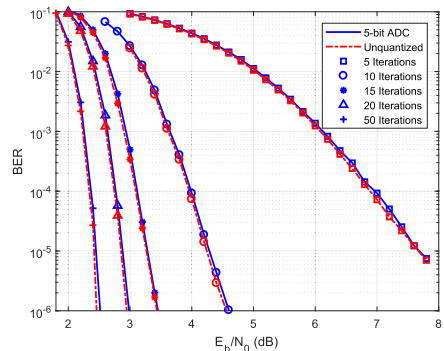


**FIGURE 11.** BER vs. iterations: AR3A Code, 10 × 10 MIMO, 10 − 50 iterations, code rate $R = 1/2$, block length: 9600 bits.
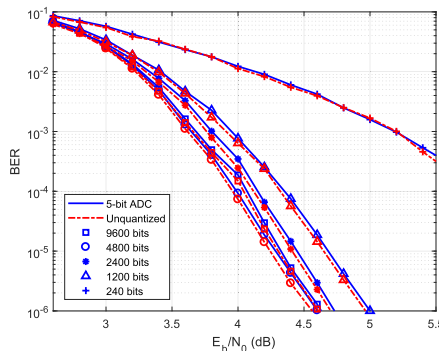


**FIGURE 13.** BER vs. block length: 10 × 10 MIMO, 10 iterations, code rate $R = 1/2$, block length: 120 bits − 9600 bits.

the modified PEXIT algorithm holds for the cases with various MIMO configurations and decoding iterations, as shown in Fig. 12 and Fig. 11. Special attention should be given to Fig. 12 where one can see that the 4-bit ADC curves approach the curve of the unquantized one when the receive antenna is

from 30 to 80. This behavior can be observed by looking at the iterative decoding threshold in Table. 5.

Fig. 13 shows the BER performance of 5-bit ADC system and the unquantized one under various code blocklength. We see that the performance gap is very tiny at all the
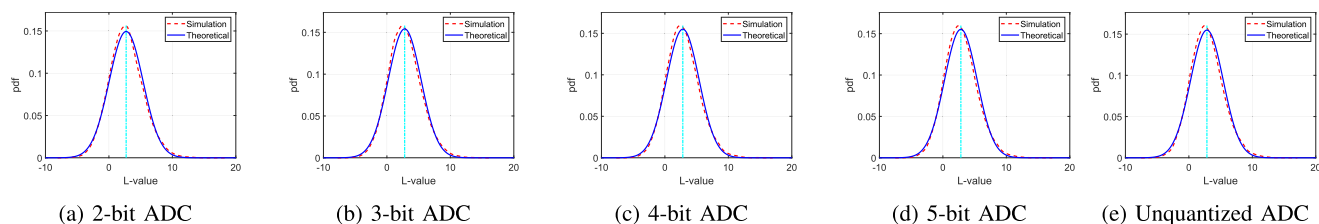
**FIGURE 14.** Pdfs of L-value at the output of the detector: AR3AR code, $10 \times 10$ MIMO, 10 iterations, code rate $R = 1/2$, blocklength: 9600 bits.
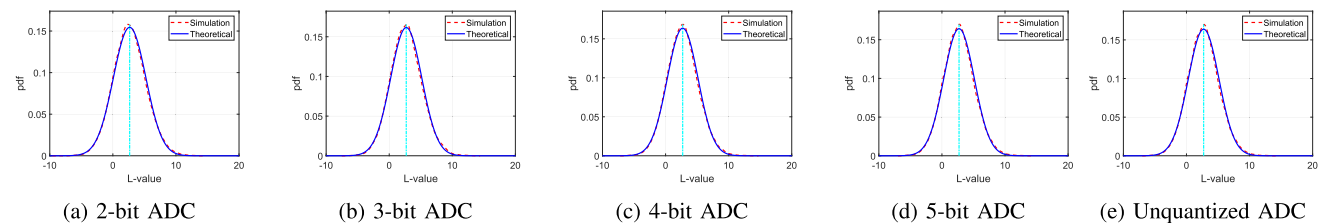


**FIGURE 15.** Pdfs of L-value at the output of the detector: AR3AR code, $20 \times 20$ MIMO, 10 iterations, code rate $R = 1/2$, blocklength: 9600 bits.
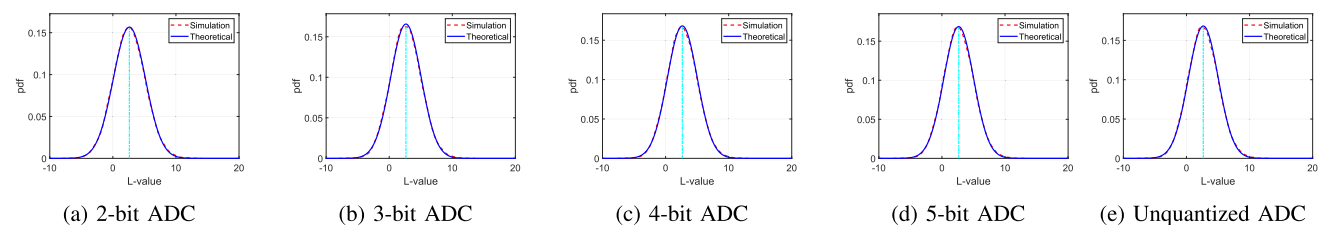


**FIGURE 16.** Pdfs of L-value at the output of the detector: AR3AR code, $30 \times 30$ MIMO, 10 iterations, code rate $R = 1/2$, blocklength: 9600 bits.
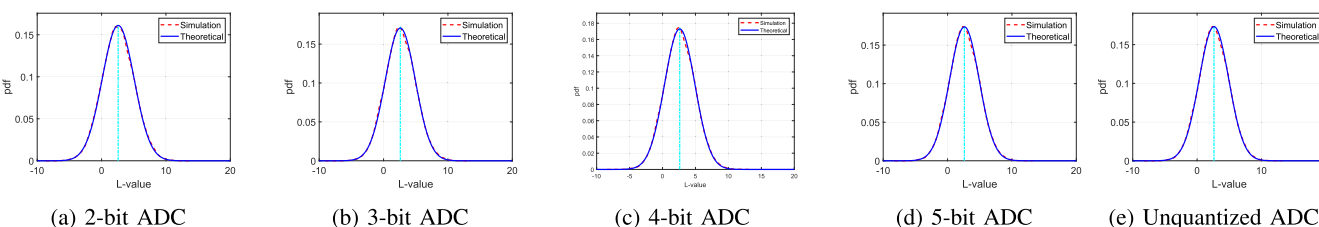


**FIGURE 17.** Pdfs of L-value at the output of the detector: AR3AR code, $100 \times 100$ MIMO, 10 iterations, code rate $R = 1/2$, blocklength: 9600 bits.

code blocklengths from 120 bits to 9600 bits. Note that the modified PEXIT algorithm is derived under the assumption that the code blocklength is infinite. However, the simulation results confirm that 5-bit ADC resolution can approach the performance of the unquantized one for short blocklengths as well.

## VII. CONCLUSION

We derived a new version of the PEXIT algorithm for LS-MIMO communications systems with low-resolution ADCs. The proposed PEXIT algorithm can predict the behavior of the protograph LDPC codes under various input parameters, including the LS-MIMO configuration, the code rate, the maximum number of iterations, and the code structure. We found that there is small performance loss when using 3-bit or 4-bit ADC resolution in comparison with the unquantized one. The performance of the 5-bit ADC system approaches that of the unquantized one in all test cases.

## REFERENCES

[1] J. Thorpe, "Low-density parity-check (LDPC) codes constructed from protographs," Jet Propuls. Lab., California Inst. Technol., Pasadena, CA, USA, IPN Progr. Rep. 42–154, 2003.

[2] Y. Fang, G. Bi, Y. L. Guan, and F. C. M. Lau, "A survey on protograph LDPC codes and their applications," IEEE Commun. Surveys Tuts., vol. 17, no. 4, pp. 1989–2016, 4th Quart., 2015.

[3] A. Yu, S. Jing, Y.-L. Ueng, X. You, and C. Zhang, "Iterative SOR detection and decoding for LDPC-coded massive MIMO systems," in Proc. 9th Int. Conf. Wireless Commun. Signal Process. (WCSP), Oct. 2017, pp. 1–5.

[4] T. L. Narasimhan and A. Chockalingam, "Exit chart based design of irregular LDPC codes for large-MIMO systems," IEEE Commun. Lett., vol. 17, no. 1, pp. 115–118, Jan. 2013.

[5] L. Fan, S. Jin, C. K. Wen, and H. Zhang, "Uplink achievable rate for massive MIMO systems with low-resolution ADC," IEEE Commun. Lett., vol. 19, no. 12, pp. 2186–2189, Oct. 2015.

[6] Q. Ding and Y. Lian, "Performance analysis of mixed-ADC massive MIMO systems over spatially correlated channels," IEEE Access, vol. 7, pp. 6842–6852, 2019.

[7] M. Srinivasan and S. Kalyani, "Analysis of massive MIMO with low-resolution ADC in Nakagami-m fading," IEEE Commun. Lett., vol. 23, no. 4, pp. 764–767, Apr. 2019.

[8] Y. Cho and S.-N. Hong, "One-bit successive-cancellation soft-output (OSS) detector for uplink MU-MIMO systems with one-bit ADCS," *IEEE Access*, vol. 7, pp. 27172–27182, 2019.

[9] J. Zhang, L. Dai, Z. He, B. Ai, and O. A. Dobre, "Mixed-ADC/DAC multipair massive MIMO relaying systems: Performance analysis and power optimization," *IEEE Trans. Commun.*, vol. 67, no. 1, pp. 140–153, Jan. 2019.

[10] D. C. Araújo, T. Maksymyuk, A. L. F. de Almeida, T. Maciel, J. C. M. Mota, and M. Jo, "Massive MIMO: Survey and future research topics," *IET Commun.*, vol. 10, no. 15, pp. 1938–1946, Oct. 2016.

[11] T. Takahashi, S. Ibi, and S. Sampei, "On normalization of matched filter belief in GABP for large MIMO detection," in *Proc. IEEE 84th Veh. Technol. Conf. (VTC-Fall)*, Sep. 2016, pp. 1–6.

[12] W. Fukuda, T. Abiko, T. Nishimura, T. Ohgane, Y. Ogawa, Y. Ohwatari, and Y. Kishiyama, "Low-complexity detection based on belief propagation in a massive MIMO system," in *Proc. IEEE 77th Veh. Technol. Conf. (VTC Spring)*, Jun. 2013, pp. 1–5.

[13] T. Van Nguyen, A. Nosratinia, and D. Divsalar, "The design of rate-compatible protograph LDPC codes," *IEEE Trans. Commun.*, vol. 60, no. 10, pp. 2841–2850, Oct. 2012.

[14] G. Liva and M. Chiani, "Protograph LDPC codes design based on EXIT analysis," in *Proc. IEEE Global Telecommun. Conf. (GLOBECOM)*, Washington, DC, USA, Nov. 2007, pp. 3250–3254.

[15] D. Divsalar, S. Dolinar, C. R. Jones, and K. Andrews, "Capacity-approaching protograph codes," *IEEE J. Sel. Areas Commun.*, vol. 27, no. 6, pp. 876–888, Aug. 2009.

[16] Y. Fang, P. Chen, L. Wang, F. C. M. Lau, and K. K. Wong, "Performance analysis of protograph-based low-density parity-check codes with spatial diversity," *IET Commun.*, vol. 6, no. 17, pp. 2941–2948, Nov. 2012.

[17] S. T. Brink, G. Kramer, and A. Ashikhmin, "Design of low-density parity-check codes for modulation and detection," *IEEE Trans. Commun.*, vol. 52, no. 4, pp. 670–678, Apr. 2004.

[18] X. Zhao, Y. Li, J. Zhong, M. Zhao, and C. Zheng, "Low-complexity layered joint detection and decoding for LDPC coded large-MIMO systems," in *Proc. Int. Conf. Wireless Commun. Signal Process.*, Oct. 2013, pp. 1–6.

[19] A. Gersho and R. M. Gray, *Vector Quantization And Signal Compression*. Norwell, MA, USA: Kluwer, 1992.

[20] J. Dai, J. Liu, J. Wang, J. Zhao, C. Cheng, and J.-Y. Wang, "Achievable rates for full-duplex massive MIMO systems with low-resolution ADCs/DACs," *IEEE Access*, vol. 7, pp. 24343–24353, 2019.

[21] D. Tse and P. Viswanath, *Fundamentals Of Wireless Communication*. Cambridge, U.K.: Cambridge Univ. Press, 2005.

[22] H. T. Nguyen, T. A. Ramstad, and I. Balasingham, "Wireless sensor communication system based on direct-sum source coder," *IET Wireless Sensor Syst.*, vol. 1, no. 2, pp. 96–104, Jun. 2011.

[23] D. Hui and D. L. Neuhoff, "Asymptotic analysis of optimal fixed-rate uniform scalar quantization," *IEEE Trans. Inf. Theory*, vol. 47, no. 3, pp. 957–977, Mar. 2001.

[24] Y. Xiong, N. Wei, and Z. Zhang, "A low-complexity iterative GAMP-based detection for massive MIMO with low-resolution ADCs," in *Proc. IEEE Wireless Commun. Netw. Conf. (WCNC)*, Mar. 2017, pp. 1–6.

[25] T. J. Richardson, M. A. Shokrollahi, and R. L. Urbanke, "Design of capacity-approaching irregular low-density parity-check codes," *IEEE Trans. Inf. Theory*, vol. 47, no. 2, pp. 619–637, Feb. 2001.

[26] T. Van Nguyen and H. T. Nguyen, "The design of optimized fast decoding protograph LDPC codes," in *Proc. Int. Conf. Adv. Technol. Commun. (ATC)*, Oct. 2016, pp. 282–286.

[27] T. Abiko, W. Fukuda, T. Nishimura, T. Ohgane, Y. Ogawa, Y. Ohwatari, and Y. Kishiyama, "An EXIT chart analysis for belief-propagation based detection in a large-scale MIMO system," in *Proc. IEEE 77th Veh. Technol. Conf. (VTC Spring)*, Jun. 2013, pp. 1–5.

[28] S. Gounai and T. Ohtsuki, "Performance analysis of LDPC code with spatial diversity," in *Proc. IEEE Veh. Technol. Conf.*, Sep. 2006, pp. 1–5.

[29] H. Uchikawa, "Design of non-precoded protograph-based LDPC codes," in *Proc. IEEE ISIT*, Jun./Jul. 2014, pp. 2779–2783.

[30] S.-N. Hong and N. Lee, "Soft-output detector for uplink MU-MIMO systems with one-bit ADCs," *IEEE Commun. Lett.*, vol. 22, no. 5, pp. 930–933, May 2018.

[31] T. Koike-Akino, D. S. Millar, K. Kojima, K. Parsons, Y. Miyata, K. Sugihara, and W. Matsumoto, "Iteration-aware LDPC code design for low-power optical communications," *J. Lightw. Technol.*, vol. 34, no. 2, pp. 573–581, Jan. 15, 2016.

[32] X.-Y. Hu, E. Eleftheriou, and D. M. Arnold, "Regular and irregular progressive edge-growth tanner graphs," *IEEE Trans. Inf. Theory*, vol. 51, no. 1, pp. 386–398, Jan. 2005.

[33] J. Hamkins, "Performance of low-density parity-check coded modulation," Jet Propuls. Lab., California Inst. Technol., Pasadena, CA, USA, IPN Prog. Rep. 42-184, Feb. 2011.

**THUY V. NGUYEN** received the B.Sc. degree from the Hanoi University of Science and Technology (HUST), Hanoi, Vietnam, the M.Sc. degree from New Mexico State University, Las Cruces, NM, USA, and the Ph.D. degree from The University of Texas at Dallas, Richardson, TX, USA, all in electrical engineering. He was a member of the Technical Staff with Flash Channel Architecture, Seagate, Fremont, CA, USA. He is currently a Lecturer of the Faculty of Information Technology, Posts and Telecommunications Institute of Technology (PTIT), Hanoi. His research interest includes coding theory and its applications in next-generation communication systems.

**HIEU D. VU** received the B.Sc. degree in electronics and telecommunications from the Hanoi University of Science and Technology and the M.Sc. degree in digital communications from Kiel University. He is currently pursuing the Ph.D. degree in electrical engineering with the Posts and Telecommunications Institute of Technology (PTIT), Hanoi, Vietnam. His current research interests include source/channel coding and wireless MIMO communications with low-resolution ADCs.

**DIEP N. NGUYEN** received the M.E. degree in electrical and computer engineering from the University of California San Diego (UCSD) and the Ph.D. degree in electrical and computer engineering from The University of Arizona (UA). He was a DECRA Research Fellow with Macquarie University and a member of technical staff with Broadcom, California, and ARCON Corporation, Boston, consulting the Federal Administration of Aviation on turning detection of UAVs and aircraft, US Air Force Research Laboratory on anti-jamming. He is currently a Faculty Member of the Faculty of Engineering and Information Technology, University of Technology Sydney (UTS). His current research interests include computer networking, wireless communications, and machine learning application, with emphasis on systems' performance and security/privacy. He has received several awards from LG Electronics, University of California at San Diego, The University of Arizona, the US National Science Foundation, and the Australian Research Council. He is an Associate Editor of the IEEE TRANSACTIONS ON MOBILE COMPUTING and a Guest Editor of IEEE ACCESS.

**HIEU T. NGUYEN** received the B.Sc. degree from the Hanoi University of Science and Technology, the M.Sc. degree from the University of Saskatchewan, Canada, and the Ph.D. degree from the Norwegian University of Science and Technology, all in electrical engineering. He is currently a Faculty Member of the Faculty of Technology, Natural Sciences, and Maritime Sciences, University of South-Eastern Norway (USN).

● ● ●